



**HAL**  
open science

## Metal-free covalent organic frameworks containing precise heteroatoms for electrocatalytic oxygen reduction reaction

Jiali Li, Ji Jia, Jinquan Suo, Cuiyan Li, Zhiwei Wang, Hui Li, Valentin Valtchev, Shilun Qiu, Xiaoming Liu, Qianrong Fang

► **To cite this version:**

Jiali Li, Ji Jia, Jinquan Suo, Cuiyan Li, Zhiwei Wang, et al.. Metal-free covalent organic frameworks containing precise heteroatoms for electrocatalytic oxygen reduction reaction. *Journal of Materials Chemistry A*, 2023, 11 (34), pp.18349-18355. 10.1039/D3TA03534D . hal-04280286

**HAL Id: hal-04280286**

**<https://hal.science/hal-04280286>**

Submitted on 10 Nov 2023

**HAL** is a multi-disciplinary open access archive for the deposit and dissemination of scientific research documents, whether they are published or not. The documents may come from teaching and research institutions in France or abroad, or from public or private research centers.

L'archive ouverte pluridisciplinaire **HAL**, est destinée au dépôt et à la diffusion de documents scientifiques de niveau recherche, publiés ou non, émanant des établissements d'enseignement et de recherche français ou étrangers, des laboratoires publics ou privés.

# Metal-Free Covalent Organic Frameworks Containing Precise Heteroatoms for Electrocatalytic Oxygen Reduction Reaction

Jiali Li,<sup>a</sup> Ji Jia,<sup>a</sup> Jinqian Suo,<sup>a</sup> Cuiyan Li,<sup>a</sup> Zhiwei Wang,<sup>b</sup> Hui Li,<sup>\*a</sup> Valentin Valtchev,<sup>c</sup> Shilun Qiu,<sup>a</sup> Xiaoming Liu,<sup>\*a</sup> and Qianrong Fang<sup>\*a</sup>

Received 00th January 20xx,  
Accepted 00th January 20xx

DOI: 10.1039/x0xx00000x

Covalent organic frameworks (COFs) have been used for electrocatalytic oxygen reduction reaction (ORR) due to their structural tunability, well-defined electroactive sites, and easy introduction of heteroatoms. Researchers have incorporated heteroatoms into COF architectures to enhance their performance by turning the electronic environment of oxygen intermediates. However, only a few heteroatoms (O, S, N, P) have been introduced into the backbone of COFs, and the effects of different types of heteroatoms on the electronic structure of COFs have not been specifically investigated. Furthermore, the development of COF electrocatalysts with highly active ORR is still at an early stage. Herein, we report a series of metal-free benzotrithiophene-based COFs containing various heteroatoms (Se, S or O), BTT-COFs (named JUC-616, JUC-617, and JUC-618, respectively), and explore their ORR catalytic activity. Remarkably, JUC-616 involving precise Se atoms exhibits a half-wave potential of 0.78 V and a high turnover frequency (TOF) of 0.0062 s<sup>-1</sup> at 0.75 V vs. reversible hydrogen electrode (RHE), which is the best among the metal- and pyrolysis-free COF-based electrocatalysts reported so far. Thus, this work promotes the promising potential of functionalized COFs with precise heteroatoms for electrocatalysts.

## Introduction

The oxygen reduction reaction (ORR) has attracted a lot of attention over the last decade as it is a key process for sustainable and green energy storage and conversion technologies such as fuel cell<sup>1</sup> and rechargeable metal-air batteries.<sup>2, 3</sup> Nevertheless, an efficient ORR process requires robust catalysts to overcome the inherently sluggish kinetics of oxygen activation and accelerate the reaction rate.<sup>4, 5</sup> Nowadays, platinum (Pt)-based nanomaterials are also the most efficient ORR catalysts, but problems such as high price, poor durability, and small Pt reserves hinder their large-scale commercial applications.<sup>6, 7</sup> Therefore, it is of great significance to develop metal-free electrocatalysts with excellent ORR performance as an alternative to Pt-containing materials. At present, heteroatoms have been shown to be a promising strategy for preparing metal-free carbon-based electrocatalysts.<sup>8</sup> By integrating different heteroatoms into different nanostructures of carbon, various metal-free heteroatom-doped carbon composites have been developed, ranging from single-atom doping (N, P, B, S, etc.) to multi-heteroatom doping (N/P/S or N/S/B, etc.).<sup>9</sup> However,

traditional heteroatom-doped carbon materials, such as heteroatom-doped carbon nanotubes, reduced graphene oxides, mesoporous carbon, etc., usually have random structures with high uncertainty,<sup>10</sup> and thus the way in which dopants promote ORR by tuning the electronic structure of effective defects is not well understood.

Covalent organic frameworks (COFs) are a new class of crystalline porous polymeric materials linked by strong covalent bonds between nodes and linkers.<sup>11, 12</sup> Since the first report by Yaghi's group in 2005,<sup>13</sup> COFs have attracted great scientific interest for applications in various fields such as catalysis,<sup>14-18</sup> energy storage,<sup>19-21</sup> optoelectronics,<sup>22-24</sup> etc.<sup>25-29</sup> owing to their large acceptable surface area, high crystallinity and structural tunability. Compared with traditional heteroatom-doped materials, COFs retain their original skeleton and crystal structure, and have fast ion transport channels and well-defined electroactive sites. More importantly, they enable precise tuning of environmental features around active sites, such as electronic properties and coordination states. The large number of heteroatoms in the COF leads to a redistribution of charges, while some positively charged atoms are more favourable for the adsorption of O<sub>2</sub> act as reaction centres.<sup>30</sup> In addition, the activity, selectivity and stability of catalysts depend on the scale, heteroatom content, doping location of active sites, and porous structure, and COFs allow precise control of these elements simultaneously due to their fixed backbone structures, which facilitates in-depth exploration of the relationship between catalyst structure and catalytic performance.<sup>31</sup> Over the past few years, preliminary explorations have shown that two-dimensional (2D) COFs can serve as promising platforms for electrocatalytic reactions.<sup>32-34</sup> Generally, a post-pyrolysis strategy is often employed

<sup>a</sup> College of Chemistry, Jilin University, Changchun 130012, China E-mail: [postlh@jlu.edu.cn](mailto:postlh@jlu.edu.cn), [xm\\_liu@jlu.edu.cn](mailto:xm_liu@jlu.edu.cn), [arfang@jlu.edu.cn](mailto:arfang@jlu.edu.cn).

<sup>b</sup> Institute of Theoretical Chemistry, College of Chemistry, Jilin University, Changchun 130023

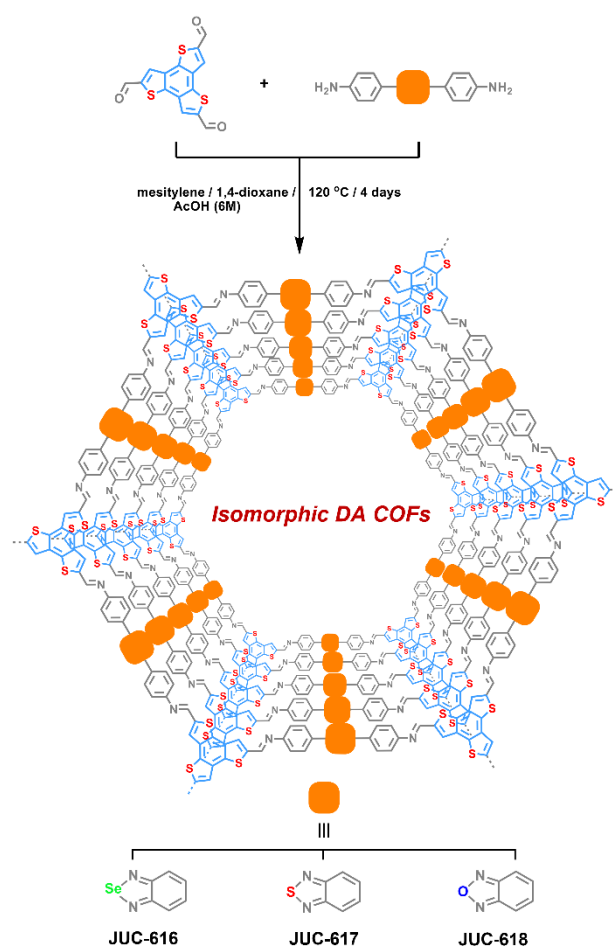
<sup>c</sup> Qingdao Institute of Bioenergy and Bioprocess Technology, Chinese Academy of Sciences; Normandie Univ, 6 Marechal Juin, 14050 Caen, France

† Electronic Supplementary Information (ESI) available: materials and characterization, SEM images, TEM images, FT-IR spectra, TGA curves, PXRD patterns, and unit cell parameters. See DOI: 10.1039/x0xx00000x

to improve the catalytic performance of COFs for ORR.<sup>35, 36</sup> However, the high-temperature treatment process usually inevitably leads to energy consumption and uncontrollable structural changes, resulting in poorly defined active sites, which limits a deep understanding of the ORR mechanism.<sup>37</sup> To avoid the hassle of pyrolysis, some pyrolysis-free COFs were recently explored and showed precise skeleton structures and accurate active sites.<sup>38-41</sup>

In 2020, we proposed for the first time to introduce S element into the framework of non-pyrolyzable COFs to precisely modulate the performance of ORR.<sup>42</sup> So far, although there are many studies on the catalytic performance of heteroatom-containing COFs for ORR, the effect of doping various heteroatoms with different electronegativity on the electronic structure of COFs is rarely reported, and the development of COFs electrocatalysts with highly active ORR is still in its infancy.<sup>43</sup> Multi-heteroatom doping is a more effective and versatile approach than single dopants,<sup>44</sup> so it is crucial to study the effect of COFs containing multiple heteroatoms on the ORR performance. However, it is common to investigate heteroatoms such as O, S, N, and P in the framework of COFs, and further exploration of atoms with higher activity is needed to investigate more active catalysts. In 2021, Han's research group introduced Se atoms to prepare Se single-atom catalysts with excellent catalytic performance, but this study led to incomplete pyrolysis structures, which hindered the precise tuning of atoms.<sup>45</sup> Se, a chalcogen element with larger atom size and high polarizability to S or O, has been shown to increase the electrical transport properties of framework materials.<sup>46, 47</sup> In addition, Se has a large atomic radius, small ionization energy, and abundant d electrons, which can facilitate charge transfer and increase the catalyst affinity for (O) OH species.<sup>48</sup> Combining the unique properties of COF materials such as high atomic utilization, pre-designed structure and easy introduction of various heteroatoms, doping Se into the COF architectures and studying its effect on ORR performance will provide a new direction for the application of COF materials in electrocatalysts.

Herein, we reported a series of novel metal-free electrocatalysts with excellent ORR performance by precisely introducing heteroatoms (Se, S, or O) into periodic benzotrithiophene-based COFs (BTT-COFs) via Schiff-base condensation reaction. Moreover, all these COFs possess a uniform porous structure with high surface area and electron donor-acceptor (D-A) characteristics, which can facilitate mass transport, expose a large number of active sites, and improve its electrical conductivity for fast electron transport.<sup>49</sup> The influence of different heteroatoms on the electronic structure of COF materials was investigated in detail by calculating the adsorbed-state differential charges and D-band differential charges of the three materials. Remarkably, the Se-containing COF showed excellent electrocatalytic performance with a half-wave potential of 0.78 V and a high turnover frequency (TOF) of 0.0062 s<sup>-1</sup> at 0.75 V vs. reversible hydrogen electrode (RHE), which is better than that of other metal- and pyrolysis-based COF electrocatalysts reported so far.



**Scheme 1.** Synthesis and chemical structures of isomorphic BTT-COFs (JUC-616, JUC-617, and JUC-618).

## Results and discussion

Selecting benzo[1,2-b:3,4-b':5,6-b''] trithiophene-2,5,8-tricarbaldehyde (BTT) with electron-donating properties as a triangular knot<sup>50</sup> and electron-accepting 4,4'-benzosenadiazole-4,7-diyl-diaminobenzene (BSD), 4,4'-benzothiadiazole-4,7-diyl-diaminobenzene (BTD) or 4,4'-benzoxadiazole-4,7-diyl-diaminobenzene (BXD) as a linear linker,<sup>51</sup> three isomorphic BTT-COFs with D-A structural features, JUC-616, JUC-617 and JUC-618, were successfully designed and synthesized by imine reversible condensation reaction under solvothermal conditions, giving brown to orange microcrystalline powders (Scheme 1, the corresponding synthesis details were given in the Supporting Information). They were insoluble in common organic solvents and water. Fourier transform infrared spectroscopy (Supporting Information, Figure S1) showed a peak located at ~1613 cm<sup>-1</sup> for all of BTT-COFs, corresponding to the formation of the imine bond. Additionally, the signals of -NH<sub>2</sub> nearly disappeared compared with their corresponding monomers, demonstrating the conversion of the amine to imine groups. The successful formation of the designed COF frameworks and the presence of imine linkage were confirmed by cross-polarization magic angle spinning (CP/MAS) <sup>13</sup>C solid-state NMR (Supporting Information, Figure

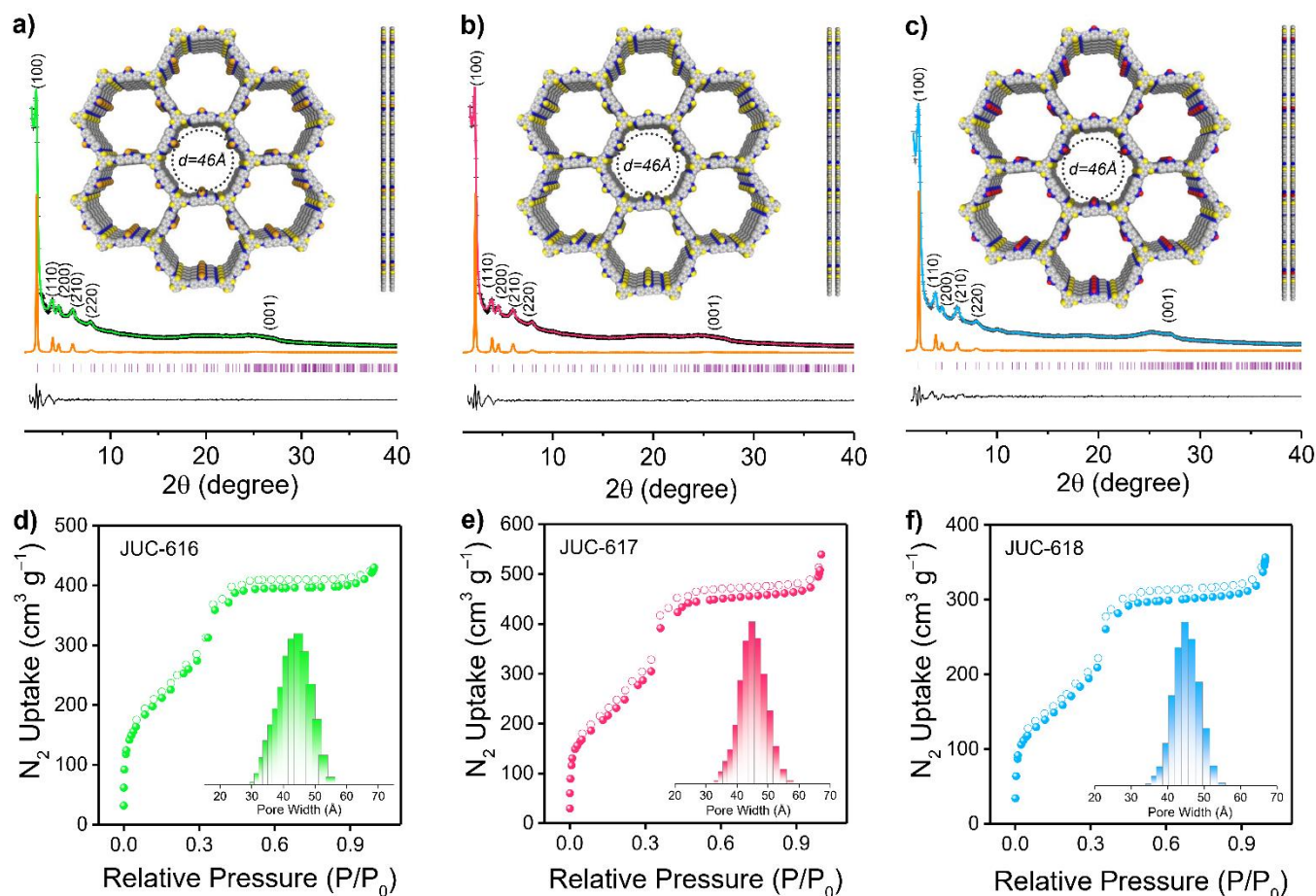


**Fig. 1.** Powder XRD patterns of JUC-616 (a), JUC-617 (b) and JUC-618 (c). The observed XRD patterns (+), Pawley refined (pink), simulation (orange), the difference between the observed and refined profiles (black) and Bragg position (green). Insets: crystal structures with AA stacking modes. Nitrogen adsorption (filled circles)-desorption (open circles) isotherms of JUC-616 (d), JUC-617 (e) and JUC-618 (f). Insets: pore size estimated using non-local density functional theory.

S2). Furthermore, X-ray photoelectron spectroscopy (XPS) was performed to verify the molecular structures of BTT-COFs. For example, the survey spectrum showed that the JUC-616 was composed of carbon, nitrogen, sulfur, and selenium (Supporting Information, Figure S3a). The XPS spectra of N1s display two distinct peaks, each exhibiting similar C=N-C binding energies of 398.6, 398.6, and 398.7 eV for the three materials, respectively. This similarity arises from the identical chemical environment of N in the imine bond.<sup>52</sup> However, the different electronegativities of O, S, and Se introduce variability in the binding energies of the second peak associated with N. Specifically, the Se-N=C peak appears at 399.1 eV in JUC-616, the S-N=C peak at 399.3 eV in JUC-617, and the O-N=C peak at 400.5 eV in JUC-618.<sup>53-55</sup> For the high-resolution S 2p spectrum of JUC-616, the binding energies at 165.3 and 164.1 eV were ascribed to C-S-C in the BTT unit.<sup>56</sup> Additionally, the peaks at 57.8 and 57.0 eV were assigned to Se 3d<sub>3/2</sub> and Se 3d<sub>5/2</sub> in the benzoselenadiazole group.<sup>57</sup> Similarly, structural characterizations of JUC-617 and JUC-618 were carried out to demonstrate their chemical composition and structure (Supporting Information, Figure S4). Thermogravimetric analysis (TGA) revealed good thermal durability of the three COFs up to 400 °C in a N<sub>2</sub> atmosphere, with less than 10% weight loss of the materials (Supporting Information, Figure S5).

The crystalline structures of the three COFs were evaluated by powder X-ray diffraction (PXRD) analysis combined with theoretical simulations. As displayed in Figure 1a-c, the experimental PXRD patterns of JUC-616, JUC-617, and JUC-618 showed a strong diffraction peak at 2.29°, which corresponds to the (100) reflection, implying the formation of long-range ordered structures. And other relatively broad peaks at about 3.96, 4.59, 6.05, 7.91, and 25.04° can be assigned to the (110), (200), (210), (220), and (001) planes, respectively. Notably, due to their isomorphous structures, the diffraction peak of the same plane of the three COFs appeared at almost the same position.<sup>58</sup> Structural simulations using Materials Studio showed that all synthesized COFs are based on AA stacking of the 2D topology of **hcg** in space group *P-6* (No.174, Supporting Information, Tables S1-S3). The PXRDs of the three COFs based on AB stacking were also calculated, showing a mismatch with the experimental PXRD patterns (Supporting Information, Figure S6). Full profile pattern matching (Pawley) refinements were performed from their PXRD patterns. The unit cell parameters were also obtained ( $a = b = 44.5786$  Å and  $c = 3.5617$  Å for JUC-616,  $a = b = 44.5873$  Å and  $c = 3.5439$  Å for JUC-617,  $a = b = 44.6085$  Å and  $c = 3.5302$  Å for JUC-618, and  $\alpha = \beta = 90^\circ$ ,  $\gamma = 120^\circ$  for all of COFs). Those results yielded unit cell parameters that closely match with the observed values with an excellent agreement factor ( $a = b =$

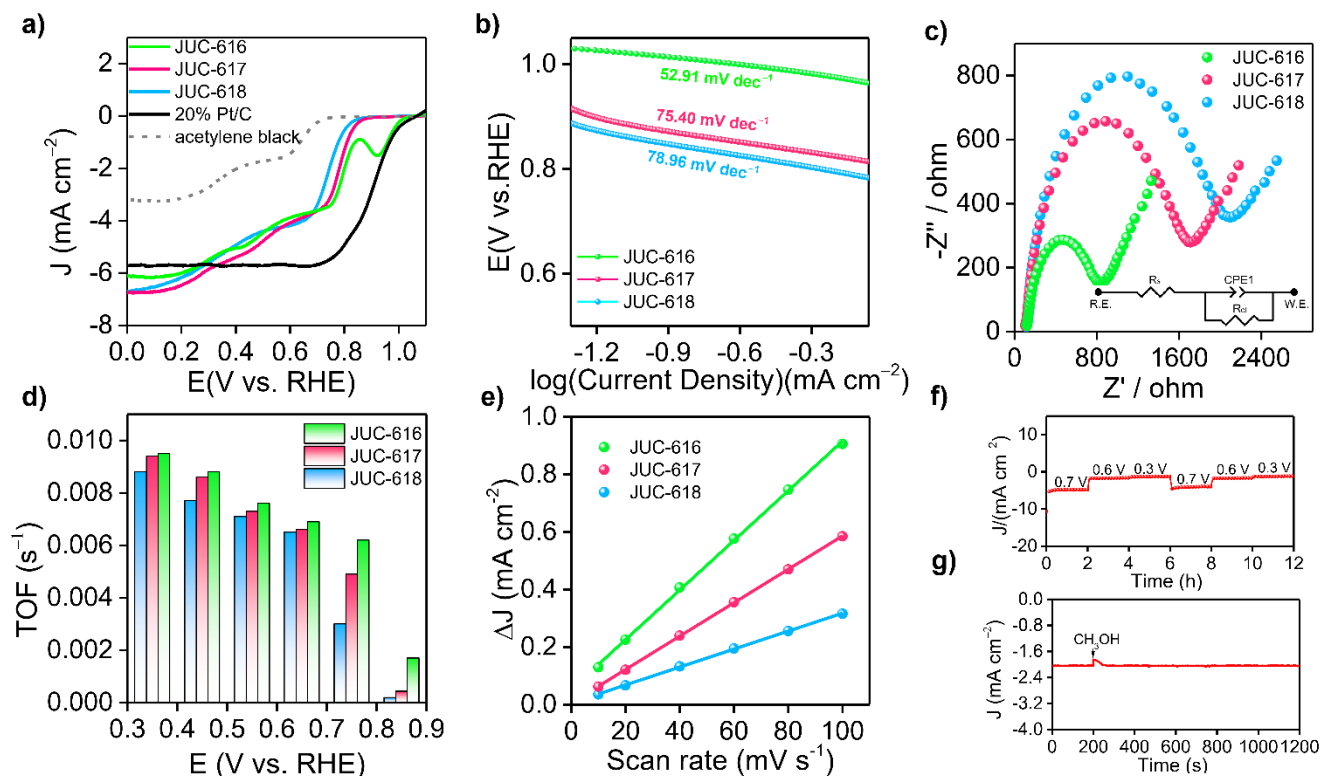


**Fig. 2.** (a) LSV curves of three isomorphous COFs in  $O_2$ -saturated 0.1 M KOH electrolyte at a scan rate of 1600 rpm. (b) Tafel plots of three COFs. (c) The impedance of COFs at open circuit voltage. Inset: equivalent circuit. (d) TOFs and mass activities of COFs. (e) Cdl values of COFs. (f) Multi-step amperometry curve of JUC-616 at an applied voltage of 0.3, 0.6 and 0.7 V. (g) Current–time curve of JUC-616 at 0.7 V vs RHE.

44.5787 Å and  $c = 3.5618$  Å,  $\alpha = \beta = 90^\circ$ ,  $\gamma = 120^\circ$  for all of COFs,  $R_{wp} = 3.23\%$ ,  $R_p = 2.45\%$  for JUC-616,  $R_{wp} = 3.09\%$ ,  $R_p = 2.19\%$  for JUC-617 and  $R_{wp} = 1.57\%$ ,  $R_p = 1.17\%$  for JUC-618, respectively).

The morphology of the BTT-COFs was studied by field-emission scanning electron microscopy (FE-SEM), which exhibits needle-like or spherical nanoclusters aggregated into coral-like masses (Supporting Information, Figure S7). In addition, high-resolution transmission electron microscopy (HR-TEM) images revealed long-range channels (Supporting Information, Figure S8), illustrating further their high crystallinity. The lattice fringes of the BTT-COFs were calculated by using the software to be 0.38 nm counter to the (001) crystal plane, which is close to the simulated layer distances (0.35 nm). Furthermore, the nitrogen adsorption–desorption isotherms of the as-synthesized COFs were performed at 77 K to estimate their porosity. As illustrated in Figure 1d–f, the sorption curves of JUC-616, JUC-617, and JUC-618 showed the type IV reversible isotherms, which is characteristic of mesoporous materials. The Brunauer–Emmett–Teller (BET) surface area was evaluated to be  $893 \text{ m}^2 \text{ g}^{-1}$  for JUC-616,  $943 \text{ m}^2 \text{ g}^{-1}$  for JUC-617, and  $630 \text{ m}^2 \text{ g}^{-1}$ , respectively. Their total pore volumes were calculated to be 0.66, 0.78, and  $0.53 \text{ cm}^3 \text{ g}^{-1}$  at  $P/P_0 = 0.99$ . Additionally, the pore size distribution calculated using non-local density functional theory (NLDFT) shows that three isomorphous COFs exhibit same homogeneous pore with a pore size of 45 Å (Figure 1d–f, insets), which matched theoretical value of 46 Å based on the AA stacking mode (Figure 1a–c, insets).

The UV-Vis diffuse reflectance spectrum (UV-DRS) of BTT-COFs displayed a broad absorption band with a tail extending to 1000 nm

(Supporting Information, Figure S9), which corresponds to their D-A structural characteristic. According to the Tauc plot, the optical bandgaps ( $E_g$ ) of JUC-616, JUC-617, and JUC-618 were evaluated to be 1.98, 2.06, and 2.08 eV, respectively (Supporting Information, Figure S10). Compared to JUC-617 and JUC-618, JUC-616 had a smaller  $E_g$ , which was more conducive to electron transmission.<sup>59, 60</sup> Based on the electrochemical Mott–Schottky spectra, we estimated the conduction band minimum (CBM) of JUC-616 to be -1.10 V vs. NHE, which is more negative than -1.04 V for JUC-617 and -0.84 V for JUC-618 (Supporting Information, Figure S11), implying a stronger electron reduction capacity of JUC-616.<sup>61</sup>

The electrocatalytic ORR performance of the obtained COFs was then evaluated at room temperature by a three-electrode system in an  $O_2$ -saturated 0.1 M KOH electrolyte at a scan rate of 1600 rpm. As depicted in Figure 2a, the linear sweep voltammetry (LSV) curves of the samples displayed that JUC-616 exhibited better ORR performance than the isomorphous JUC-617 and JUC-618, which clearly indicated the importance of introducing Se atoms into the skeleton to enhance the ORR activity. The electrocatalytic ORR activity of COFs was verified by cyclic voltammetry (CV), and compared with JUC-617 (0.73 V) and JUC-618 (0.70 V), JUC-616 exhibited the highest electrochemical ORR activity with an oxygen reduction peak at 0.74 V vs. RHE (Supporting Information, Figure S12). The half-wave potential of JUC-616 was 0.78 V vs. RHE, which was more positive than JUC-617 (0.73 V vs. RHE) and JUC-618 (0.70 V vs. RHE). Furthermore, the limiting current densities of the three isomorphous COFs were close to  $6.0 \text{ mA cm}^{-2}$ , indicating that their mass transfer is almost identical due to their similar pore structures,

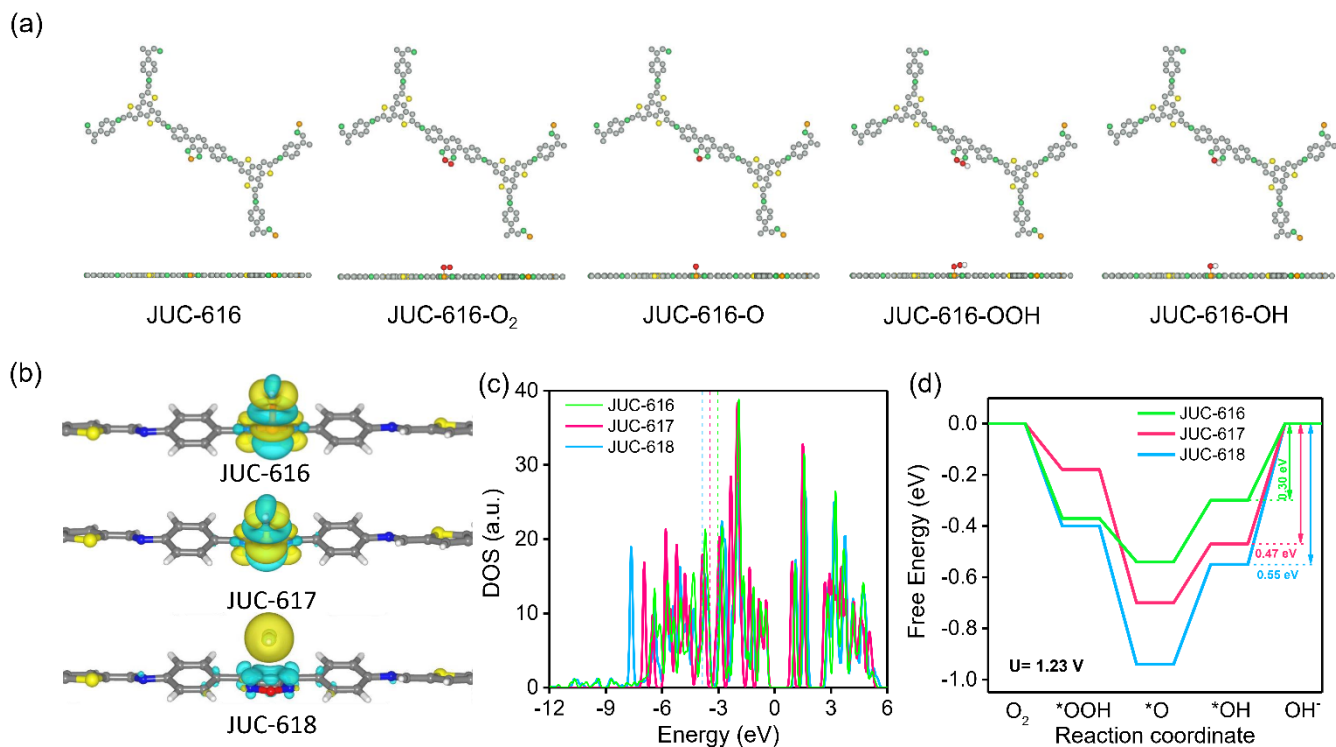


**Fig. 3.** (a) Models for the adsorption of different ORR reaction intermediates by JUC-616. The grey, green, yellow, red, orange and white spheres represent C, N, S, O, Se and H atoms, respectively. (b) The charge distribution of JUC-616. The curly, silvery white, green and yellow spheres represent C, N, Se and S atoms, respectively. Free energy diagrams of Se, S, O atoms in JUC-616, JUC-617 and JUC-618 at the applied potentials of 0 V (c) and 1.23 V (d), respectively.

surface areas, and morphologies. Surprisingly, we noticed that the ORR performance of JUC-616 was outstanding among the state-of-the-art metal-free COFs reported without a pyrolysis process (Supporting Information, Table S4). As shown in Figure 2b, the Tafel slope of JUC-616 was determined to be 52.91 mV dec<sup>-1</sup>, which is smaller than that of JUC-617 (75.40 mV dec<sup>-1</sup>) and JUC-618 (78.96 mV dec<sup>-1</sup>), thus revealing the faster ORR kinetics of Se-containing JUC-616 (Supporting Information, Figure S13). Obviously, the changing trend of the obtained Tafel slope value is consistent with the result of LSV curve. Additionally, electrochemical impedance spectroscopy (EIS) measurements were performed on the obtained COFs to evaluate their conductive properties. Accordingly, the charge transfer resistances of JUC-616, JUC-617, and JUC-618 were 769, 1600, and 1941 Ω, respectively (Figure 2c), which indicated that JUC-616 had a faster electron transfer capability. The electron transfer number (*n*) of JUC-616, JUC-617, and JUC-618, calculated from Koutecky-Levich (K-L) plots, were 3~3.8 in the potential range of 0.2-0.6 V vs. RHE (Figure 2d, Supporting Information Figures S14-S15, and Table S5), suggesting a four-electron pathway in the ORR process.<sup>62</sup> Similar to the K-L equation, the electron transfer number (*n*) of JUC-616, JUC-617, and JUC-618 from the rotating ring disk experiments, were 3~3.7 in the potential range of 0.0-0.7 V vs. RHE (Supporting Information, Figure S16).

Next, the origin of the high performance of JUC-616 was also discussed from the experimental point of view. A linear relationship between electrochemically active surface areas (ECSAs) and double layer capacitance (C<sub>dl</sub>) is well known.<sup>63</sup> Therefore, C<sub>dl</sub> was performed by the CV method (Supporting Information, Figure S17). As shown in Figure 2e, the C<sub>dl</sub> for JUC-616 is 8.62 mF cm<sup>-2</sup>, which is larger than 5.80 mF cm<sup>-2</sup> of JUC-617, 3.12 mF cm<sup>-2</sup> of JUC-618, and

7.6 mF cm<sup>-2</sup> of JUC-528 with bithiophene-sulfur structure,<sup>42</sup> indicating that the Se-containing COF can provide more efficient active sites. The intrinsic activity of materials was investigated by calculating the conversion frequency (TOF) at various potentials. As shown in Figure 2d, JUC-616 has the largest TOF value at different potentials, which promotes the adsorption and desorption of O<sub>2</sub> and products on the catalyst surface.<sup>64</sup> These obtained results clearly demonstrate that Se-containing JUC-616 shows the highest electrocatalytic ORR active among the three isomorphous COFs. In addition, as shown in Figure 2f, multi-step chronoamperometry measurements were also conducted at potentials of 0.3, 0.6, and 0.7 V, and the experimental data revealed that the current density of JUC-616 remained almost constant at each applied potential throughout the experimental cycle, indicating that JUC-616 has high electrochemical stability in alkaline solution.<sup>65</sup> A negligible loss for the current density was found when adding methanol into the electrolyte at 0.7 V vs. RHE (Figure 2g), proving the good methanol tolerance of JUC-616. Comparative analysis of the three materials before and after electrocatalysis revealed that both their structure and morphology remained essentially unaltered. This observation serves as compelling evidence of the high stability exhibited by these materials throughout the electrocatalytic process (Supporting Information, Figures S18 and S19).

To further explore the catalytic activity sites and mechanism of Se-doped COF, theoretical calculations were carried out using the density functional theory (DFT) method. In order to more intuitively visualize the effects of O, S, and Se on the ORR process, we performed theoretical calculations using O, S, and Se as the active sites. The Calculation of the Mulliken charge of BTT-COFs identified the active sites as O, S and Se on the diazole, which are more prone

to nucleophilic reactions favoring the ORR reaction (Supporting Information, Figures S20 and Table S6). In addition, by calculating the differential charge of the adsorbed state, it is shown that Se and S have a strong adsorption on OH\*, proving that S and Se are the active sites. Electron transfer from COFs to OH\* intermediate during ORR can also be visualized in the charge difference map. As shown in Figure 3a, the yellow and cyan isosurfaces represent electron-rich and depleted regions, respectively. Obviously, there is no bonding or charge transfer between OH\* and JUC-618, while Se and S atoms of BSD and BTD units in JUC-616 and JUC-617 lose electrons and OH\* gains electrons. In contrast, the charge transfer between OH\* and JUC-616 and JUC-617 is large. Density of states calculations were performed for the O, S, and Se atoms in the three materials, and the DOS of their P<sub>z</sub> orbitals were calculated (Figure 3c, and Supporting Information, Figure S21), exhibiting the binding energy of the P<sub>z</sub> band center to the reaction intermediate. Compared with JUC-617 (-3.44 eV) and JUC-618(-3.81 eV), JUC-616 has higher P<sub>z</sub> band center and is more capable of binding to reaction intermediates (-3.06 eV), thus exhibiting higher activity, similar to the trend of activity predicted by “d band theory”.<sup>66,67</sup> Additionally, three adsorption intermediate models were constructed, as shown in Figures 3a and S16 in Supporting Information, and for four-electron transfer, we have calculated the free energies and overpotentials of ORR on BTT-COFs and determined the rate-limiting step. The free energy diagram of ORR (Figure 3c) indicates that the rate-limiting step of ORR is the transformation of OH\* to OH<sup>-</sup> by all COFs in the last step of ORR. According to the ΔG diagrams in Figure 3d, the highest energy barrier of the three isomorphous COFs for electrocatalytic ORR occurs in the process from OH\* to OH<sup>-</sup>, where Se-doped JUC-616 shows a lower energy barrier of 0.30 eV than JUC-617 (0.47 eV) and JUC-618 (0.55 eV). Additionally, JUC-616 has the lowest overpotential of 0.37 eV (Supporting Information, Table S7), indicating that it is more favorable for ORR reaction.

## Conclusions

In summary, a series of metal-free BTT-based COFs were designed and synthesized via the reversible condensation of imines under solvothermal conditions. They have high crystallinity, intrinsic porosity, and electron donating and accepting properties. As a metal- and pyrolysis-free electrocatalyst, JUC-616 exhibited excellent ORR activity with a half-wave potential of 0.78 V (vs. RHE), and a Tafel slope of 52.91 mV dec<sup>-1</sup>, which are better than those of previously reported COF materials. Theoretical and experimental results demonstrated that the Se atoms in the skeleton of COFs could serve as highly active sites for electrocatalytic ORR. We further highlight that this work is the first report on improving the ORR activity of COFs via Se-containing strategy, which facilitates the rational design and application of COF-based electrocatalysts. Therefore, this work develops a general strategy to enrich structural diversity of COF materials and promotes their potential applications.

## Conflicts of interest

There are no conflicts to declare.

## Acknowledgements

This work was supported by National Key R&D Program of China (2022YFB3704900 and 2021YFF0500500), National Natural Science Foundation of China (22025504, 21621001, and 22105082), the SINOPEC Research Institute of Petroleum Processing, “111” project (BP0719036 and B17020), China Postdoctoral Science Foundation (2020TQ0118 and 2020M681034), the program for JLU Science and Technology Innovative Research Team.

## References

- 1 I. Staffell, D. Scamman, A. Velazquez Abad, P. Balcombe, P. E. Dodds, P. Ekins, N. Shah and K. R. Ward, *Energy Environ. Sci.*, 2019, **12**, 463-491.
- 2 C.-Y. Su, H. Cheng, W. Li, Z.-Q. Liu, N. Li, Z. Hou, F.-Q. Bai, H.-X. Zhang and T.-Y. Ma, *Adv. Energy Mater.*, 2017, **7**, 1602420.
- 3 H. Wang, C. Tang, B. Wang, B. Li and Q. Zhang, *Adv. Mater.*, 2017, **29**, 1702327.
- 4 Z. W. Seh, J. Kibsgaard, C. F. Dickens, I. Chorkendorff, J. K. Nørskov and T. F. Jaramillo, *Science*, 2017, **355**, eaad4998.
- 5 A. Kulkarni, S. Siahrostami, A. Patel and J. K. Nørskov, *Chem. Rev.*, 2018, **118**, 2302-2312.
- 6 A. Chen and P. Holt-Hindle, *Chem. Rev.*, 2010, **110**, 3767-3804.
- 7 M. K. Debe, *Nature*, 2012, **486**, 43-51.
- 8 Z. Zhao, B. Wang, Z. You, Q. Zhang, W. Song and X. Long, *Small*, 2023, **19**, 2207298.
- 9 X. Feng, Y. Bai, M. Liu, Y. Li, H. Yang, X. Wang and C. Wu, *Energy Environ. Sci.*, 2021, **14**, 2036-2089.
- 10 K. Chalapat, N. Chekurov, H. Jiang, J. Li, B. Parviz and G. S. Paraoanu, *Adv. Mater.*, 2013, **25**, 1-1.
- 11 P. J. Waller, F. Gándara and O. M. Yaghi, *Acc. Chem. Res.*, 2015, **48**, 3053-3063.
- 12 Y. Song, Q. Sun, B. Aguila and S. Ma, *Adv. Sci.*, 2019, **6**, 1801410.
- 13 A. P. Côté, A. I. Benin, N. W. Ockwig, M. O'keeffe, A. J. Matzger and O. M. Yaghi, *Science*, 2005, **310**, 1166-1170.
- 14 Z. Zhang, J. Jia, Y. Zhi, S. Ma and X. Liu, *Chem. Soc. Rev.*, 2022, **51**, 2444-2490.
- 15 Z. Li, J. Wang, S. Ma, Z. Zhang, Y. Zhi, F. Zhang, H. Xia, G. Henkelman and X. Liu, *Appl. Catal. B Environ.*, 2022, **310**, 121335.
- 16 F. Chen, X. Guan, H. Li, J. Ding, L. Zhu, B. Tang, V. Valtchev, Y. Yan, S. Qiu and Q. Fang, *Angew. Chem. Int. Ed.*, 2021, **60**, 22230-22235.
- 17 Q. Fang, S. Gu, J. Zheng, Z. Zhuang, S. Qiu and Y. Yan, *Angew. Chem. Int. Ed.*, 2014, **53**, 2878-2882.
- 18 F. Tan, Y. Zheng, Z. Zhou, H. Wang, X. Dong, J. Yang, Z. Ou, H. Qi, W. Liu, Z. Zheng and X. Chen, *CCS Chem.*, 2022, **4**, 3751-3761.
- 19 Y. Zhang, J. Duan, D. Ma, P. Li, S. Li, H. Li, J. Zhou, X. Ma, X. Feng and B. Wang, *Angew. Chem. Int. Ed.*, 2017, **56**,

- 16313-16317.
- 20 S. Wang, Q. Wang, P. Shao, Y. Han, X. Gao, L. Ma, S. Yuan, X. Ma, J. Zhou, X. Feng and B. Wang, *J. Am. Chem. Soc.*, 2017, **139**, 4258-4261.
- 21 Y. Du, H. Yang, J. M. Whiteley, S. Wan, Y. Jin, S. H. Lee and W. Zhang, *Angew. Chem. Int. Ed.*, 2016, **55**, 1737-1741.
- 22 E. Jin, M. Asada, Q. Xu, S. Dalapati, M. A. Addicoat, M. A. Brady, H. Xu, T. Nakamura, T. Heine, Q. Chen and D. Jiang, *Science*, 2017, **357**, 673-676.
- 23 H. Ding, J. Li, G. Xie, G. Lin, R. Chen, Z. Peng, C. Yang, B. Wang, J. Sun and C. Wang, *Nat. Commun.*, 2018, **9**, 5234.
- 24 A. C. Jakowetz, T. F. Hinrichsen, L. Ascherl, T. Sick, M. Calik, F. Auras, D. D. Medina, R. H. Friend, A. Rao and T. Bein, *J. Am. Chem. Soc.*, 2019, **141**, 11565-11571.
- 25 K. Geng, T. He, R. Liu, S. Dalapati, K. T. Tan, Z. Li, S. Tao, Y. Gong, Q. Jiang and D. Jiang, *Chem. Rev.*, 2020, **120**, 8814-8933.
- 26 X. Guan, F. Chen, Q. Fang and S. Qiu, *Chem. Soc. Rev.*, 2020, **49**, 1357-1384.
- 27 W. Xian, P. Zhang, C. Zhu, X. Zuo, S. Ma and Q. Sun, *CCS Chem.*, 2021, **3**, 2464-2472.
- 28 M. Hao, Z. Chen, X. Liu, X. Liu, J. Zhang, H. Yang, G. I. N. Waterhouse, X. Wang and S. Ma, *CCS Chem.*, 2022, **4**, 2294-2307.
- 29 Y. Liu, J. Ren, Y. Wang, X. Zhu, X. Guan, Z. Wang, Y. Zhou, L. Zhu, S. Qiu, S. Xiao and Q. Fang, *CCS Chem.*, 2022, **0**, 1-13.
- 30 Y. Wang, M. Jiao, W. Song and Z. Wu, *Carbon*, 2017, **114**, 393-401.
- 31 M. Liu, S. Liu, C. Cui, Q. Miao, Y. He, X. Li, Q. Xu and G. Zeng, *Angew. Chem. Int. Ed.*, 2022, **61**, e202213522.
- 32 Y. Yusran, Q. Fang and V. Valtchev, *Adv. Mater.*, 2020, **32**, 2002038.
- 33 X. Zhao, P. Pachfule and A. Thomas, *Chem. Soc. Rev.*, 2021, **50**, 6871-6913.
- 34 D. Yang, Y. Tao, X. Ding and B. Han, *Chem. Soc. Rev.*, 2022, **51**, 761-791.
- 35 Z. Xiang, D. Cao, L. Huang, J. Shui, M. Wang and L. Dai, *Adv. Mater.*, 2014, **26**, 3315-3320.
- 36 Q. Xu, Y. Tang, X. Zhang, Y. Oshima, Q. Chen and D. Jiang, *Adv. Mater.*, 2018, **30**, 1706330.
- 37 S. Tao and D. Jiang, *CCS Chem.*, 2021, **3**, 2003-2024.
- 38 S. Royuela, E. Martínez-Periñán, M. P. Arrieta, J. I. Martínez, M. M. Ramos, F. Zamora, E. Lorenzo and J. L. Segura, *Chem. Commun.*, 2020, **56**, 1267-1270.
- 39 L. Zhai, S. Yang, X. Yang, W. Ye, J. Wang, W. Chen, Y. Guo, L. Mi, Z. Wu, C. Soutis, Q. Xu and Z. Jiang, *Chem. Mater.*, 2020, **32**, 9747-9752.
- 40 S. Chang, C. Li, H. Li, L. Zhu and Q. Fang, *Chem. Res. Chin. Univ.*, 2022, **38**, 396-401.
- 41 J. Yue, Y. Wang, X. Wu, P. Yang, Y. Ma, X. Liu and B. Tang, *Chem. Commun.*, 2021, **57**, 12619-12622.
- 42 D. Li, C. Li, L. Zhang, H. Li, L. Zhu, D. Yang, Q. Fang, S. Qiu and X. Yao, *J. Am. Chem. Soc.*, 2020, **142**, 8104-8108.
- 43 C. Yang, S. Tao, N. Huang, X. Zhang, J. Duan, R. Makiura and S. Maenosono, *ACS Appl. Nano Mater.*, 2020, **3**, 5481-5488.
- 44 J. P. Parakowitsch, J. Zhang, D. Su, A. Thomas and M. Antonietti, *Adv. Mater.*, 2010, **22**, 87-92.
- 45 H. Hu, J. Wang, B. Cui, X. Zheng, J. Lin, Y. Deng and X. Han, *Angew. Chem. Int. Ed.*, 2022, **61**, e202114441.
- 46 A. Abouimrane, D. Dambournet, K. W. Chapman, P. J. Chupas, W. Weng and K. Amine, *J. Am. Chem. Soc.*, 2012, **134**, 4505-4508.
- 47 B. Zhang, J. Zhang, F. Zhang, L. Zheng, G. Mo, B. Han and G. Yang, *Adv. Funct. Mater.*, 2020, **30**, 1906194.
- 48 H. Liang, L. Jia, F. Chen, S. Jing and P. Tsiakaras, *Appl. Catal. B Environ.*, 2022, **317**, 121698.
- 49 X. Cui, L. Gao, R. Ma, Z. Wei, C. Lu, Z. Li and Y. Yang, *J. Mater. Chem. A*, 2021, **9**, 20985-21004.
- 50 Z. Li, Z. Zhang, R. Nie, C. Li, Q. Sun, W. Shi, W. Chu, Y. Long, H. Li and X. Liu, *Adv. Funct. Mater.*, 2022, **32**, 2112553.
- 51 Z. Li, S. Han, C. Li, P. Shao, H. Xia, H. Li, X. Chen, X. Feng and X. Liu, *J. Mater. Chem. A*, 2020, **8**, 8706-8715.
- 52 D. Yan, Z. Wang, P. Cheng, Y. Chen and Z. Zhang, *Angew. Chem.*, 2021, **60**, 6055-6060.
- 53 N. Zheng, Y. Feng, Y. Zhang, R. Li, C. Bian, L. Bao, S. Du, H. Dong, Y. Shen and W. Feng, *ACS Appl. Mater. Inter.*, 2019, **11**, 24360-24366.
- 54 L. Guo, Y. Niu, S. Razzaque, B. Tan and S. Jin, *ACS Catal.*, 2019, **9**, 9438-9445.
- 55 S.-X. L. Luo, R. Y. Liu, S. Lee and T. M. Swager, *J. Am. Chem. Soc.*, 2021, **143**, 10441-10453.
- 56 W.-R. Cui, Y.-J. Li, Q.-Q. Jiang, Q. Wu, R.-P. Liang, Q.-X. Luo, L. Zhang, J. Liu and J.-D. Qiu, *Cell Rep. Phys. Sci.*, 2022, **3**, 100630.
- 57 T. Zhang, T. Cai, W. Xing, T. Li, B. Liang, H. Hu, L. Zhao, X. Li and Z. Yan, *Energy Storage Mater.*, 2021, **41**, 667-676.
- 58 R. Chen, Y. Wang, Y. Ma, A. Mal, X. Gao, L. Gao, L. Qiao, X. Li, L. Wu and C. Wang, *Nat. Commun.*, 2021, **12**, 1354.
- 59 B. He, G. Li, J. Li, J. Wang, H. Tong, Y. Fan, W. Wang, S. Sun and F. Dang, *Adv. Energy Mater.*, 2021, **11**, 2003263.
- 60 S. Bai, T. Li, H. Wang, L. Tan, Y. Zhao and Y. Song, *Chem. Eng. J.*, 2021, **419**, 129390.
- 61 T. Tian, X. Jin, N. Guo, H. Li, Y. Han and Y. Yuan, *Appl. Catal. B Environ.*, 2022, **308**, 121227.
- 62 J. Zhang, L. Qu, G. Shi, J. Liu, J. Chen and L. Dai, *Angew. Chem. Int. Ed.*, 2016, **55**, 2230-2234.
- 63 W. Huang, J. Li, X. Liao, R. Lu, C. Ling, X. Liu, J. Meng, L. Qu, M. Lin, X. Hong, X. Zhou, S. Liu, Y. Zhao, L. Zhou and L. Mai, *Adv. Mater.*, 2022, **34**, 2200270.
- 64 W. Moschkowitsch, O. Lori and L. Elbaz, *ACS Catal.*, 2022, **12**, 1082-1089.
- 65 H. Zhang, P. Li, S. Chen, F. Xie and D. J. Riley, *Adv. Funct. Mater.*, 2021, **31**, 2106835.
- 66 J. K. Nørskov, F. Abild-Pedersen, F. Studt and T. Bligaard, *PNAS*, 2011, **108**, 937-943.
- 67 S. Zhou, W. Pei, Y. Zhao, X. Yang, N. Liu and J. Zhao, *NPJ Comput. Mater.*, 2021, **7**, 186.